

## Paradoxical Brownian Motion in a Microfluidic Device: Absolute Negative Mobility

Ralf Eichhorn<sup>1</sup>, Alexandra Ros<sup>2</sup>, Jan Regtmeier<sup>2</sup>, Thanh Tu Duong<sup>2</sup>, Peter Reimann<sup>1</sup>  
and Dario Anselmetti<sup>2</sup>

<sup>1</sup> *Condensed Matter Theory, Bielefeld University, Germany*

<sup>2</sup> *Experimental Biophysics & Applied Nanoscience, Bielefeld University, Germany*

### Abstract

We report on a paradoxical migration mechanism in a microstructured lab-on-a-chip environment. The phenomenon is based on a subtle interplay between Brownian motion (thermal noise), a periodic and symmetric microstructure, and a biased AC electric field. The resulting non-linear dynamics far from thermal equilibrium gives rise to absolute negative mobility, i.e. a migrational transport, which is – both for negative and positive bias – always opposite to the net acting force, in very good agreement between experiment and theory.

## 1 INTRODUCTION

Noise effects in technological applications are mostly considered as nuisance. Their amazing benefits are being unraveled only since recently, e.g. in the context of stochastic resonance [1,2], noise suppression by noise [3], or Parrondo's paradoxical games [4]. In particular, channeling and exploiting the unavoidable thermal fluctuations is a thriving new paradigm in the field of nanosciences with fascinating applications, including transport and separation of colloidal particles [5–9] and biomolecules [10–13] by utilizing ratchet and steric effects. In this paper, we focus on a migration mechanism different from ratchet effects, which is called *absolute negative mobility* (ANM).

When applying a static force to a system at rest, a net motion opposite to that force – termed absolute negative mobility (ANM)<sup>1</sup> – seems impossible due to Newton's second law. Yet, such a paradoxical response phenomenon has been observed experimentally in semiconductor devices [14, 15] and has been predicted theoretically in simplified stochastic model systems [16–18]. To reconcile ANM with Newton's law, a non-linear dynamics is indispensable, and to avoid conflicts with the second law of thermodynamics, the system needs to operate far from equilibrium. Here, we present a more detailed account of our brief note [19], demonstrating the proof-of-principle for ANM in a microstructured lab-on-a-chip environment with potential application to (bio)analytical purposes like separation, fractionation and sorting of colloids, biomolecules and cells.

---

<sup>1</sup>As opposed to ANM, *differential* negative mobility refers to motion that slows down with increasing force.

## 2 ANM IN A MICROFLUIDIC DEVICE

The main component of our microfluidic device is its topographically structured middle section with periodically arranged rows of rectangular posts separated by alternating “small” and “large” gaps (see figure 1a). The microdevice is cast with poly(dimethylsiloxane) (PDMS) and can be filled with aqueous buffer solutions through two reservoirs at its extremities. Electric fields can be applied along the channel axis via platinum electrodes that are immersed into the reservoirs. Negatively charged polystyrene microbeads of  $2\ \mu\text{m}$  diameter are suspended in the buffer solution in low concentration so that particle-particle interactions are negligible. Particle diameter and gap widths have been chosen such that the beads can pass through the large gaps but not through the small ones (see figure 1a). The microbeads are characterized by a diffusion coefficient

$$D_{\text{eff}} = 0.63 \cdot 10^{-13} \text{ m}^2/\text{s}, \quad (2.1)$$

and a voltage dependent particle velocity in  $x$ -direction

$$v_0 = U \cdot 2.3 \cdot 10^{-7} \text{ m/Vs} \quad (2.2)$$

corresponding to a free anodic mobility of  $\mu_0 = 2.5 \cdot 10^{-9} \text{ m}^2/\text{Vs}$ , where  $U$  denotes the static voltage applied to the electrodes. Both (2.1) and (2.2) have been experimentally determined by real-time video microscopy of the particle motion between two subsequent rows of posts and averaging over a large number of particles. The direction of the  $x$ -axis relative to the sign of the electric voltage in figure 1a has implicitly been defined via (2.2) such as that a positive voltage generates positive forces along the  $x$ -axis, and analogously for negative voltages.

The device is driven away from thermal equilibrium by an unbiased AC voltage  $U_{\text{AC}}(t)$ . Due to the symmetry of the AC-drive and the microstructure, no preferential direction of net motion for the microbeads should be observed, which was experimentally verified. This setup represents our unperturbed non-equilibrium system at rest. Accordingly, the observable of foremost interest is the average migration velocity in  $x$ -direction

$$v = \left\langle \lim_{t \rightarrow \infty} \frac{x(t) - x(0)}{t} \right\rangle \quad (2.3)$$

in response to a static perturbation  $U_{\text{DC}}$  superimposed on the AC-voltage  $U_{\text{AC}}(t)$ . Experimentally, the long-time- and ensemble-average in (2.3) is approximated by observing about 40 microbeads over 4 periods of the AC-driving via real-time optical video microscopy. Repeating the procedure for different values of the static perturbation  $U_{\text{DC}}$  yields the experimental response characteristics in figure 2. The remaining experimental uncertainty is mostly due to the limited number of recorded beads, but also deviations from strictly spatially periodic conditions, and bead-to-bead variations of size and surface charge.

The pivotal feature of the response curve in figure 2 is the negative slope symmetrically around the origin – the distinct and unambiguous signature of ANM. Indeed, for not too large static voltages  $U_{\text{DC}}$  the microbeads are always moving in the direction opposite to the corresponding static forces along the  $x$ -axis, both for positive and negative  $U_{\text{DC}}$ . Increasing  $U_{\text{DC}}$  to larger static voltages, the velocity in the “wrong” direction slows down, passes through zero, and finally points in the “normal” direction, i.e. in accordance with the sign of the static forces.

### 3 THEORETICAL MODEL AND PHYSICAL MECHANISM FOR ANM

Theoretically, the motion of a single bead in the periodic microstructure is modeled by the overdamped (friction coefficient  $\gamma$ ), stochastic Langevin dynamics

$$\gamma \dot{\vec{r}} = \vec{F}(\vec{r}) + q_{\text{eff}} \vec{E}_*(\vec{r}) [U_{\text{AC}}(t) + U_{\text{DC}}]/U_* + \sqrt{2\gamma^2 D_{\text{eff}}} \vec{\xi}(t), \quad (3.1)$$

where  $\vec{r} = (x(t), y(t))$  denotes the position of the bead in the  $x$ - $y$ -plane; the remaining quantities are defined and explained with the following discussion.

The model (3.1) is based on several assumptions: (i) thermal fluctuations can be described by Gaussian white noises  $\vec{\xi}(t) = (\xi_x(t), \xi_y(t))$  with  $\langle \xi_\alpha(t) \rangle = 0$ ,  $\langle \xi_\alpha(t) \xi_\beta(s) \rangle = \delta_{\alpha\beta} \delta(t-s)$  ( $\alpha, \beta \in \{x, y\}$ ); (ii) hydrodynamic interactions between particle and microstructure are negligible apart from the effective diffusion (2.1) and mobility (2.2); (iii) the (trivial) dynamics in the vertical direction ( $z$ -axis, see figure 1) decouples from that in the horizontal directions ( $x$ - $y$ -plane); (iv) microstructure and particle boundaries are hard walls, represented by the effective constraining force  $\vec{F}(\vec{r})$  in (3.1); (v) the buffer solution is a perfect (electric) conductor and the microstructure material poly(dimethylsiloxane) is a perfect insulator. Exploiting the latter assumption, the inhomogeneous electric field within the microstructure, caused by a voltage applied to the electrodes in figure 1, can be determined by solving Laplace's equation with Neumann boundary conditions at the borders between buffer and microstructure and periodic boundary conditions along the  $y$ -axis (cf. figure 1). Along the  $x$ -axis, a preset potential difference over several spatial periods is imposed and the resulting "central unit cell" periodically continued.

By this procedure, the force field  $q_{\text{eff}} \vec{E}_*(\vec{r})$  in (3.1), generated by a constant reference voltage  $U_*$ , is obtained up to an unknown gauge factor between experimental and theoretical potential energy differences. This gauge factor contains the unknown (effective) charge  $q_{\text{eff}}$  of the bead as well as the unknown potential drop generated between subsequent rows of posts when the reference voltage  $U_*$  is applied to the electrodes. It can be determined by reproducing the experimental measurement of the free mobility (2.2) by numerical simulations on the computer. Closer inspection shows that the so computed force field, illustrated by the grey arrows in figure 3, approximates the one generated by the actual electrode configuration very well.

In a microfluidic environment, like our device in Fig. 1, the force  $q_{\text{eff}} \vec{E}_*(\vec{r})$  represents the electrophoretic effects on the particle. In this context, the quantity  $q_{\text{eff}}$  is only loosely related to the surface charge of the bead [20]. Furthermore, the electric fields typically generate a fluid flow due to electroosmosis, with the consequence that the suspended bead experiences an additional force from the streaming fluid. Modelling this effect would usually require an additional force term in (3.1). However, since our microfluidic device fulfills the requirements for similitude between electrophoresis and electroosmosis [21], we can conclude that the force field  $q_{\text{eff}} \vec{E}_*(\vec{r})$  effectively also takes into account this (quite small) electroosmotic effects. This is automatically guaranteed by our above described fit of the relevant effective  $q_{\text{eff}}$ .

The theoretical velocities (2.3) resulting from numerical simulations of (3.1) are shown as solid curve in figure 2. Within the experimental uncertainty, the agreement with the measured data is very good. Having thus established the reliability of our stochastic model dynamics (3.1), the basic mechanism responsible for the observed ANM can be readily understood, see figure 3. In fact, this intuitive picture was the starting point of our present work, followed by the numerics and finally the experiment.

## 4 EXPERIMENTAL METHODS

### 4.1 Microdevice fabrication

The microfluidic device is fabricated as reported previously [22]. Briefly, photoresist SU-8 (5) (Microresist, Germany) is spin coated on a Si-wafer (CrysTec, Germany), exposed through a chromium mask (Photronics, Germany) with a flood exposure unit (Model 8011, Oriel, USA) and developed. On this master wafer, PDMS (Sylgard 184 from Dow Corning, USA) is poured in a 1:10 ratio of curing agent to pre-polymer and cured for 4 h at 85°C. PDMS is then peeled off the wafer and cut in adequate pieces for microchip assembly. Next, the PDMS microstructure with access holes for fluid reservoirs and the cover slabs are treated with an oxygen plasma for 20 s and brought into contact to ensure tight sealing and to provide sufficient hydrophilicity for instantaneous filling with buffer solution. Finally, the entire PDMS chip is mounted on an objective slide (Menzel, Germany) for microscopy. The microstructure geometry, in particular the exact gap sizes, is determined by electron microscopy.

### 4.2 Particles and microstructure pretreatment

Microstructures are pre-treated with the poly(ethyleneoxide)-poly(propyleneoxide)-poly(ethyleneoxide) triblock copolymer F108 (generous gift from BASF, Germany) at 100  $\mu$ M concentration in 100 mM phosphate buffer pH=8.2 for 2 h. This treatment significantly reduces electroosmosis induced by negative charges on oxidized PDMS and eliminates particle adsorption in the microstructure. Carboxyl modified polystyrene particles (CML microbeads) of 2  $\mu$ m diameter (Interfacial Dynamics Corporation, USA) are diluted in 100 mM phosphate buffer pH=8.2 and washed thoroughly by centrifugation at 16400 rpm. The beads are initially filled into the microstructure hydrodynamically.

### 4.3 Measurements

Alternating voltages are applied via two Pt-electrodes, connected to two power supplies (Model MCN 14-2000 and MCN 140-1250, FUG, Germany) and controlled via a relais circuit and a Labview program. Microbead migration is observed at room temperature by video microscopy with a CCD camera (Sensicam, LaVision, Germany) on an inverted microscope (Axiovert 200, Zeiss, Germany) equipped with an automatized  $x/y$ -stage (99S008, Ludl Electronic Products, USA) using a  $\times 20$  objective (LD Achromat Plan 20  $\times$  /0,40korr, Zeiss, Germany) and visible transmitting illumination. Drift velocities are determined by analyzing video data with ImageJ freeware and Plugin MTrack2 (Nico Stuurman, University of California, San Francisco).

## 5 CONCLUSIONS

We experimentally demonstrated and theoretically analyzed the proof-of-principle for the occurrence of absolute negative mobility (ANM) – the net motion opposite to a static force of whatever direction – in a microfluidic device. Interestingly, the phenomenon of ANM is based on the existence of noise, on the other hand, its main limiting factor so far is the *weakness* of the thermal noise, making the experimental implementation of more elaborate theoretical predictions often prohibitively slow. Hence, the most promising and natural next step will be to speed up thermal diffusion by employing smaller particles, especially single biomolecules like DNA and globular proteins. This will require substantially different migration mechanisms and corresponding microstructures than in our present work, but such alternative concepts for

point-like particles have already been developed in theory for simplified model systems [17,18] and we are presently in the course of adapting them to our given experimental possibilities.

Apart from its fundamental interest as a paradoxical conspiracy of disequilibrium, non-linearity, and thermal noise, ANM may open promising new perspectives for bioanalytical applications. Since the ANM-effect depends on the diffusivity and free mobility of the particles, we expect that under identical experimental conditions different particle species respond differently to the external perturbation. Specifically, particles of different sizes may even be steered into opposite directions by suitably tailoring the DC- and AC-voltages. Such selective ANM could be exploited for efficient and flexible separation of micrometer-sized colloidal particles but also biological compounds of comparable size, like cells or cell organelles thanks to the fact that our experiment operates under biological buffer conditions. Further major advantages of this approach are its easy and cheap massive parallelization and the possibility to change the separation criteria on-line by modifying the externally applied driving signal.

We gratefully acknowledge financial support from the Deutsche Forschungsgemeinschaft within the Collaborative Research Project 613 (project D2) and RE 1344/3-1, and the ESF-program STOCHDYN.

## References

- [1] K. Wiesenfeld, F. Moss, *Nature* **373**, 33 (1995).
- [2] L. Gammaitoni, P. Hänggi, P. Jung, F. Marchesoni, *Rev. Mod. Phys.* **70**, 223 (1998).
- [3] J. M. G. Vilar, J. M. Rubi, *Phys. Rev. Lett.* **86**, 950 (2001).
- [4] G. P. Harmer, D. Abbott, *Nature* **402**, 864 (1999).
- [5] J. Rousselet., L. Salome, A. Ajdari, J. Prost, *Nature* **370**, 446 (1994).
- [6] L. P. Faucheux, A. Libchaber, *Faraday Trans.* **91**, 3163 (1995).
- [7] L. Gorre-Talini, J. P. Spatz, P. Silberzan, *Chaos* **8**, 650 (1998).
- [8] C. Marquet, A. Buguin, L. Talini, P. Silberzan, *Phys. Rev. Lett.* **88**, 168301-1-4 (2002).
- [9] S. Matthias, F. Müller, *Nature* **424**, 53 (2003).
- [10] J. Han, H. G. Craighead, *Science* **288**, 1026-1029 (2000).
- [11] J. S. Bader *et al.*, *PNAS* **96**, 13165-13169 (1999).
- [12] L. Huang, E. Cox, R. H. Austin, J. Sturm, *Anal. Chem.* **75**, 6963-6967 (2003).
- [13] A. van Oudenaarden, S. G. Boxer, *Science* **285**, 1046-1048 (2001).
- [14] T. J. Banys, I. V. Parshelyunas, Y. K. Pozhela, *Sov. Phys. Semicond.* **5**, 1727 (1972) [*Fiz. Tekh. Poluprovodn.* **5** (1971) 1990].
- [15] B. J. Keay *et al.*, *Phys. Rev. Lett.* **75**, 4098 (1995).
- [16] P. Reimann, R. Kawai, C. Van den Broeck, P. Hänggi, *Europhys. Lett.* **45**, 545 (1999).
- [17] R. Eichhorn, P. Reimann, P. Hänggi, *Brownian Motion Phys. Rev. Lett.* **88**, 190601 (2002).
- [18] B. Cleuren, C. Van den Broeck, *Phys. Rev. E* **67**, 055101 (2003).
- [19] A. Ros, R. Eichhorn, J. Regtmeier, T. Duong, P. Reimann, D. Anselmetti, *Nature* **436**, 928 (2005).
- [20] D. Long, J.-L. Viovy, A. Ajdari, *Phys. Rev. Lett.* **76**, 3858 (1996).
- [21] E. B. Cummings, S. K. Griffiths, R. H. Nilson, P. H. Paul, *Anal. Chem.* **72**, 2526 (2000).
- [22] T. Duong *et al.*, *Microelectr. Eng.* **67-68**, 905 (2003).

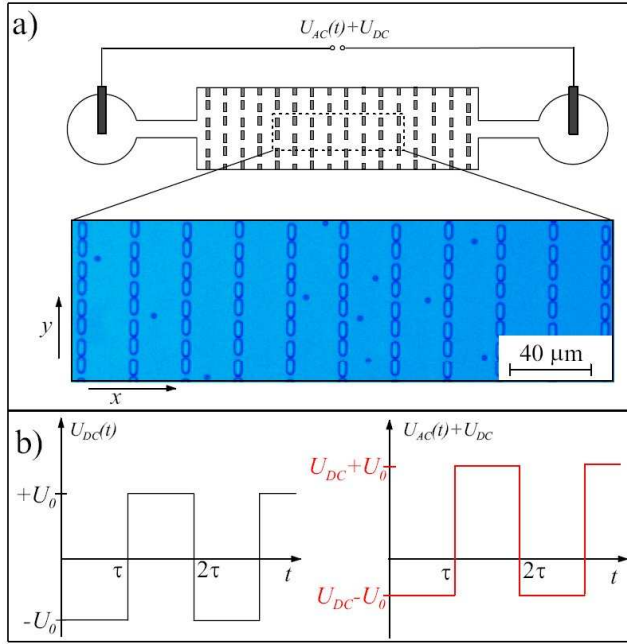


**Fig. 1.** (a) Schematic top view ( $x$ - $y$ -plane) of the experimental setup (not to scale). Electrodes are immersed into the two reservoirs of 2 mm diameter. Those are connected by inlet and outlet channels (each of length  $2500 \mu\text{m}$  and cross section  $24 \mu\text{m} \times 9 \mu\text{m}$  with the central, microstructured part. It extends over  $6000 \mu\text{m} \times 400 \mu\text{m}$  in the  $x$ - $y$ -plane and  $9 \mu\text{m}$  in height ( $z$ -direction) and contains periodically arranged posts (obstacles). The enlargement shows a partial view (optical micrograph image) of the posts (bright, rectangular) and the migrating microbeads (dark dots) of  $2 \mu\text{m}$  diameter. In each row of posts the gaps are alternately smaller ( $1.7 \pm 0.1 \mu\text{m}$ ) and larger ( $3.1 \pm 0.1 \mu\text{m}$ ) than the bead diameter. The row distance is  $(22.5 \pm 0.1) \mu\text{m}$ . Along the  $x$ -axis, the gaps are in line and again alternately large and small. An alternating voltage  $U_{AC}(t)$  (left curve in (b), switching periodically between  $\pm U_0$  with period  $2\tau$ ), is applied to the electrodes, resulting in an unbiased non-linear bead-dynamics far from thermal equilibrium. Superimposing a static DC voltage  $U_{DC}$  on top of the AC drive gives rise to a biased total voltage as indicated by the right curve in (b).

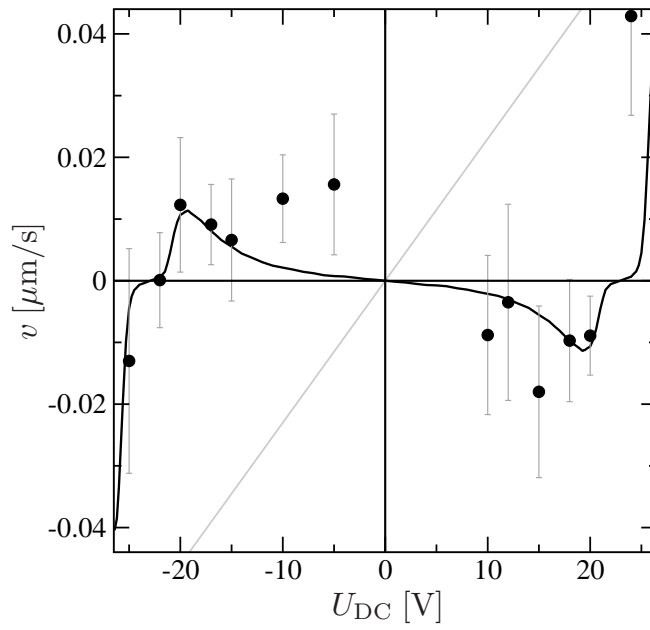


**Fig. 2.** Absolute negative mobility of  $2\mu\text{m}$  beads in the microfluidic device as specified in figure 1 for an amplitude  $U_0 = 30\text{ V}$  and a switching time  $\tau = 25\text{ s}$  of the AC-voltage. Dots with error bars: Experimentally observed average migration velocity (2.3) versus DC-voltage. Solid black curve: Theoretical response characteristics obtained from numerical simulations as detailed in the main text. Straight grey line: “normal” response behavior in the absence of AC-drive and micro-posts. Depicted is the approximation (2.2) with  $v = v_0/100$ .

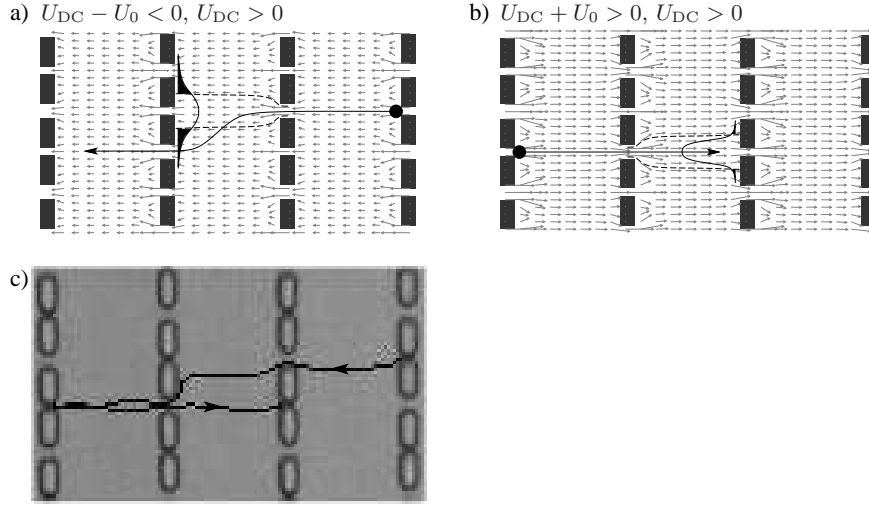


**Fig. 3.** Intuitive explanation of absolute negative mobility for a positive static DC voltage  $U_{\text{DC}}$  on top of the AC drive, as illustrated by the right curve in figure 1b. (a) Schematic motion of a microbead (black dot) in the microstructure from figure 1a (dark rectangles) during any half-period of duration  $\tau$  with total voltage  $U_{\text{DC}} - U_0 < 0$ ,  $U_{\text{DC}} > 0$ . The grey arrows indicate direction and magnitude of the corresponding force field (see main text for its detailed computation). Though the field is spatially inhomogeneous, the  $x$ -component of the force always points in the same (negative) direction as the total voltage. While the field lines can pass through the small gaps between the posts, the bead cannot. Hence these gaps act as deterministic “traps”. For one of them, the border of the attraction basin is indicated by dashed lines. Once the bead is trapped by a small gap, the probability to escape by thermal noise is negligible. In order to avoid such a trap, the particle has to pass by thermal diffusion over the dashed basin-boundary during its traveling time from one row of posts to the next. The probability of doing so is indicated by the tails of the distribution of an ensemble of beads which started out in the adjacent large gap to the right. (b) Motion of the microbead during a subsequent half-period of duration  $\tau$  with total voltage  $U_{\text{DC}} + U_0 > 0$ ,  $U_{\text{DC}} > 0$ . Since  $U_{\text{DC}} > 0$ , the total voltage and hence the forces are larger in modulus than in (a) and of opposite sign. Accordingly, the traveling time from one row of posts to the next is shorter and the diffusive dispersion narrower. Likewise, the probability to avoid a trap is smaller than in (a) and hence the average traveling distance smaller. The overall result is a net motion in the negative  $x$ -direction, i.e. opposite to the positive static DC voltage. (c) Experimentally observed particle trajectory during one driving period  $2\tau$ , illustrating the theoretical explanation of absolute negative mobility in (a) and (b).